

Implicitly Defined Layers in Neural Networks

Q. Zhang

Y. Gu

M. Michalkiewicz

M. Baktashmotlagh

A. Eriksson

University of Queensland (qianggong.zhang@uq.edu.au)

Abstract

In conventional formulations of multilayer feedforward neural networks, the individual layers are customarily defined by explicit functions. In this paper we demonstrate that defining individual layers in a neural network implicitly provide much richer representations over the standard explicit one, consequently enabling a vastly broader class of end-to-end trainable architectures. We present a general framework of implicitly defined layers, where much of the theoretical analysis of such layers can be addressed through the implicit function theorem. We also show how implicitly defined layers can be seamlessly incorporated into existing machine learning libraries. In particular with respect to current automatic differentiation techniques for use in backpropagation based training. Finally, we demonstrate the versatility and relevance of our proposed approach on a number of diverse example problems with promising results.

1. Introduction

Conventional multi-layer neural networks are exclusively defined through *explicit* expressions of its entering layers and loss functions. These expressions are typically provided in the form of a function mapping the input $y^{(k)}$ of the k -th layer to its output $y^{(k+1)}$, as

$$y^{(k+1)} = f(y^{(k)}). \quad (1)$$

Here $y^{(k)}$ may contain the output of the previous layer as well as the trainable parameters¹. This explicit approach has the advantage that training through back-propagation, a method that operates on the partial derivatives associated with each layer, is straightforward to implement. However, this approach has also proven to be rather restrictive in that the types of layers that can be included in end-to-end trainable networks is limited. The aim of this work is to show that defining individual layers *implicitly* provide much richer representations over the standard explicit one, consequently enabling a vastly broader class of end-to-end trainable architectures.

¹commonly denoted θ .

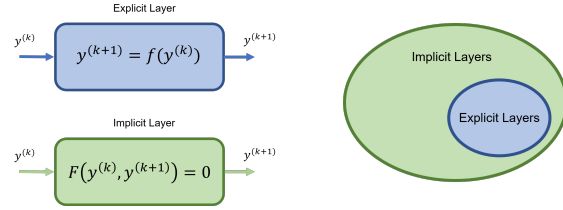


Figure 1: Explicitly vs implicitly defined layers (left). The latter enables a broader class of end-to-end trainable networks (right).

By an implicit layer we mean a layer that is defined implicitly by an implicit equation, that is

$$0 = F(y^{(k)}, y^{(k+1)}). \quad (2)$$

An intuition into why this reformulation is beneficial can perhaps be found in multivariable calculus, where the notion of *functions given by a formula* has invariably been seen as too limited for many purposes. There are countless examples of functions that cannot be expressed explicitly, for instance the locus of the expression

$$y^5 + 16y - 32x^3 + 32x = 0 \quad (3)$$

defines a precise and sketchable subset of \mathbb{R}^2 yet no formula for it exists. As feedforward layers are conceptually functions mapping the input onto the output, a similar conclusion can also be made here, that is, not all implicit layers can be expressed explicitly. The reverse, however, is indeed true, all explicit layers can be expressed implicitly. This follows trivially as any explicit layer in the form $y^{k+1} = f(y^k)$ can be defined implicitly as $y^{k+1} - f(y^k) = 0$. Hence the set of implicit layers is a proper superset of the set of explicit layers, fig. 1.

The main contributions of this paper are as follows.

- We present a general framework of implicitly defined layers, enabling a much broader class of end-to-end trainable networks. We show that much of the theoretical analysis of such layers can be addressed through the implicit function theorem.

- We show how implicitly defined layers can be seamlessly incorporated into existing machine learning libraries. In particular we prove how our framework is directly applicable to current automatic differentiation techniques for use in backpropagation based training.
- We demonstrate the versatility and practical benefit of our proposed approach on a number of diverse example problems.

2. Related works

Optimization plays a key role in a wide array of machine learning applications as a tool to perform inference in learning. Differentiation through optimization problems (e.g. argmin operators) has seen a number of advances in recent years, among which, there are techniques that come up in bi-level optimization [13, 19] and sensitivity analysis [4, 16, 22].

More specifically, [19] proposed semi-smooth Newton algorithms that could efficiently find optimal regularization parameters, leading to efficient learning algorithms. The proposed bi-level learning framework could be applied to variational models, including the non-smooth functions, but not including data fidelity terms that are different from quadratic ones. The authors of [13] presented results for differentiating parameterised argmin and argmax optimization problems through equality constraints, but did not consider inequality constraints, and thus could only be applied to a limited class of problems with smooth functions within the argmin and argmax domain. The work of [22] considered argmin differentiation for a dictionary learning problem, and presents an efficient algorithm to solve it.

Moreover, [3] considered argmin differentiation within the context of the bundle method, and learned the inference step along with the network itself, without building structured prediction architectures explicitly. [16] used implicit differentiation on convex objectives with coordinate subspace constraints but was unable to cope with general linear equality constraints and inequality constraints.

All the aforementioned approaches have limited applications in a sense that they either consider equality constraints in their implicit differentiation [13, 19] rather than both equality and inequality constraints, or they can only insert the optimisation problem in the final layer of the network [16].

Most closely related to our work is the recent method of [2], in which, the implicit differentiation can be performed through both inequality and equality constraints, and the optimisation problems can be inserted anywhere in the network. To derive the gradients from the KKT matrix of the optimisation problem, OptNet [2] makes use of techniques from matrix differential calculus. However, this work is restricted to convex quadratic problems only.

The work presented here differs to these existing works in that we are proposing a more general framework applicable to any layer expressible as an implicit function. Furthermore, most of the above mentioned work requires manual derivations and implementation of analytic gradient expressions, whereas in our framework this is not needed.

3. The Implicit Layer

In this work we present a principled treatment of *implicitly* defined layers in feedforward neural networks. We formally define this concept as follows.

Definition 1 (Implicit Layer). *A neural network layer is implicitly defined if its output $y^{(k+1)} \in \mathbb{R}^m$ is given as the solution of the k system of equations, with $F : \mathbb{R}^n \times \mathbb{R}^m \mapsto \mathbb{R}^m$,*

$$F(y^{(k)}, y^{(k+1)}) = 0, \quad (4)$$

for some input $y^{(k)} \in \mathbb{R}^n$.

We distinguish this from the usual explicitly defined feedforward layers where this relationship between input and output is given as $y^{(k+1)} = f(y^{(k)})$. As before, $y^{(k)}$ does not only denote the output of the previous layer but also the trainable parameters of the current layer.

3.1. The Implicit Function Theorem

To overcome the limitations of the naive definition of functions as explicit expressions, functions are instead commonly defined in a set-theoretic sense [14].

Here a function f from a set X to a set Y is formally defined as a set of ordered pairs (x, y) , $x \in X$ and $y \in Y$ with the properties that (i) for each $x \in X$ there exist a pair $(x, y) \in f$. (ii) If both $(x, y) \in f$ and $(x, y') \in f$ then $y = y'$. With this definition each $x \in X$ defines a unique $y \in Y$ for which $(x, y) \in f$. That is, it describes the process of associating each element of X with a single unique element in Y . It is common to use the more convenient notation of letting $y = f(x)$ denote $(x, y) \in f$.

The system of equations in (4) define an arbitrary closed (if F is continuous) subset of \mathbb{R}^l . And although no explicit expression might exist, it can be shown that under certain conditions such implicit expressions can be *locally* expressed as functions (with the above definition). The details of sufficient conditions for this to hold is provided by the *Implicit Function Theorem* [18], see thm. 1. This theorem states that under certain mild conditions on the partial derivatives the solution to a system such as (4) is locally the graph of a function. Note that these functions might also only be available implicitly. However, this theorem goes on to say that if such functions exist they must be continuously differentiable and that their derivatives can have a simple analytical expression. It is this latter consequence of the

implicit function theorem that much of the results in paper will build on.

Theorem 1 (Implicit Function Theorem). *Given three open sets $X \subseteq \mathbb{R}^n, Y \subseteq \mathbb{R}^m$, and $Z \subseteq \mathbb{R}^m$, if function $F : X \times Y \mapsto Z$ is continuously differentiable, and $(\hat{x}, \hat{y}) \in \mathbb{R}^n \times \mathbb{R}^m$ is a point for which*

$$F(\hat{x}, \hat{y}) = 0, \quad (5)$$

and the Jacobian of F with respect to $y \subseteq Y$

$$J_{F,y} \Big|_{i,j} = \left[\frac{\partial F_i}{\partial y_j} \right] \quad (6)$$

is invertible at (\hat{x}, \hat{y}) , then there exists an open set $W \subseteq \mathbb{R}^n$ with $x \in W$ and a unique continuously differentiable function $\phi : W \mapsto Z$ such that $y = \phi(x)$ and

$$F[x, y] = 0 \quad (7)$$

holds for $x \in W$.

In addition, it can be shown that the partial derivatives of ϕ in W are given by

$$\frac{\partial y}{\partial x_l} = - [J_{F,y}]^{-1} \left[\frac{\partial F}{\partial x_l} \right], \quad (8)$$

which leads to the compact form

$$J_{y,x} = - [J_{F,y}]^{-1} [J_{F,x}]. \quad (9)$$

Next we will show how an implicitly defined layer can be realised and incorporated into a trainable feedforward network, mainly through the application of the above theorem.

3.2. Backpropagation in Implicit Layers

We will assume that an implicit definition of the layer in question is given along with a method for performing a forward pass, that is, a solver of (4). The most appropriate choice here is highly task specific, examples of different forward methods are given in section 4. Note that our proposed framework is entirely agnostic to the choice of forward method.

The remaining question then relates to the backward pass through the implicit layer. To form a backward pass of a neural network layer we require the partial derivatives of its output with respect to its input, including the previous layer's output and all the trainable parameters of this layer. Hence, we need an expression for all these partial derivatives and an efficient way to calculate them. We will show that the former is provided by the implicit function theorem and the latter can be obtained by utilising existing auto-differentiation techniques.

3.2.1 The Backward Pass

Unlike in conventional neural networks pipelines, the forward and the backward path of an implicit layer are independent, which means the formulation of the functions in the forward path does not have to be the same as in the backward path. In fact, our proposed framework is entirely agnostic to the choice of forward pass. Here the backward pass of an implicit layer is obtained as follows. Let the current state of the layer be given by $(\hat{y}^{(k)}, \hat{y}^{(k+1)})$ such that $F(\hat{y}^{(k)}, \hat{y}^{(k+1)}) = 0$. Our premise is that there then exists, in the set-theoretic sense, a function $\phi : \mathbb{R}^m \mapsto \mathbb{R}^n$ such that $y^{(k+1)} = \phi(y^{(k)})$ and that ϕ is differentiable in some neighbourhood of $(\hat{y}^{(k)}, \hat{y}^{(k+1)})$. Let the partial Jacobian of F with respect to the output $y^{(k+1)}$ be denoted by

$$J_{F,y^{(k+1)}} \Big|_{i,j} = \left[\frac{\partial F_i}{\partial y_j^{(k+1)}} \right] \quad (10)$$

Then from the the implicit function theorem, thm 1, it follows directly that if $J_{F,y^{(k+1)}}$ has full rank at $(\hat{y}^{(k)}, \hat{y}^{(k+1)})$ then our assertion will hold that, a differentiable ϕ exists and is given by

$$J_{y^{(k+1)},y^{(k)}} = - [J_{F,y^{(k+1)}}]^{-1} [J_{F,y^{(k)}}], \quad (11)$$

evaluated in some neighbourhood of $(\hat{y}^{(k)}, \hat{y}^{(k+1)})$.

3.3. Automatic Differentiation

Techniques for *algorithmic differentiation* or *automatic differentiation* in machine learning has contributed significantly to the progress of deep learning methods, in large parts thanks to the development and application of back-propagation to the training of multi-layer neural networks. These techniques provide accurate, efficient, and reliable computation of partial derivatives in a fully automated manner. Thus, eliminating the need for manual derivation and implementation of analytical gradient formulae. This task can be prohibitively time consuming, particularly in situations where the models or network architecture is expected to change frequently. In this section we show how existing implementations can be used to provide backward passes through implicitly defined layers with little modification.

Let our implicit layer be defined as in (4) by $F(y^{(k)}, y^{(k+1)}) = 0$. Now consider the related explicit layer defined by

$$z^{(k+1)} = F(z^{(k)}), \quad z^{(k)} \in \mathbb{R}^{n+m}, \quad z^{(k+1)} \in \mathbb{R}^m \quad (12)$$

As this layer is defined explicitly we can apply existing automatic differentiation methods directly, providing us with the partial derivatives

$$\frac{\partial z_i^{(k+1)}}{\partial z_j^{(k)}} = \frac{\partial F_i}{\partial z_j^{(k)}}, \quad i \in [1, m], \quad j \in [1, m+n] \quad (13)$$

If we now let $z_j^{(k)} = [y_j^{(k)}, y_i^{(k+1)}]$ and $z_j^{(k+1)} = 0$ then (31) can be partitioned as

$$\frac{\partial z^{(k+1)}}{\partial z^{(k)}} = \begin{bmatrix} J_{F,y^{(k+1)}} & \Big| & J_{F,y^{(k)}} \end{bmatrix} \quad (14)$$

with $0 = F(z^{(k)})$. Comparing (14) with (11) we observe that the required terms for calculating the backward pass are provided by automatic differentiation of (31). Consequently, the automatic differentiation of implicit layers can be realised as a matrix inversion and multiplication, with no need for manual derivation or model specific implementations.²

4. Application Showcases

In this section we present four showcases of employing implicit layers in end-to-end neural network pipelines. We provide two examples that solves an argmin problem. One is hand written digits recognition on MNIST; we use an implicit layer to model a Quadratic Programming (QP) process with the same QP formulation as in [2]. The other argmin example is graph matching that matches landmarks across images; we solve the underlying relaxed Quadratic Assignment Problem (QAP) [5] with an implicit layer. The third example is image segmentation where an implicit layer performs a Normalised Cut [29] using generalised eigenvalue calculations on the Laplacian. The last example demonstrates using an implicit layer to represent and infer 3D shape using a Level Set formulations [10, 24, 9].

Note, our intent here is not to propose new methods for solving specific tasks nor attempting to beat state-of-the-art algorithms. Rather, the purpose of introducing these examples is to demonstrate the generality of our proposed formulations, how uncomplicated it is to incorporate implicit layers with existing machine learning libraries and finally to showcase the practical versatility of our framework.

4.1. QP layer on MNIST

Differentiation through optimization problems is an active topic for years [13, 19, 2, 16, 22]. Amongst these works, OptNet [2] is one of the first that analytically differentiates through both inequality and equality constraints, however limited to quadratic problems only. In this introductory showcase, We intentionally keep the formulation of the QP problem, as well as the structure of network, the same as in [2] to facilitate a transparent comparison. In particular, we demonstrate how an implicit QP layer (as well as an OptNet’s QP layer) works in a hand written digits recognition pipeline on the MNIST dataset.

Fig. 2 shows the pipeline. Two fully connected layers take input from the vectorised 28×28 image and output x ($|x| = 10$), followed by a QP solving layer that outputs

y^* ($|y^*| = 10$), which is the optimal solution of the QP problem, and finally, y^* goes through softmax and yields the negative log likelihood loss.

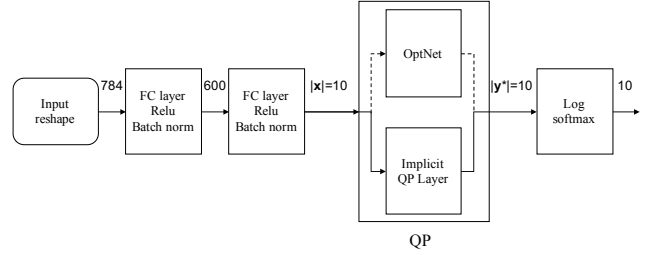


Figure 2: The hand written digits recognition pipeline. The solid branch and the dashed one in the QP module respectively represent using implicit QP layer and OptNet’s QP layer.

Now we show the KKT conditions form the implicit-function system that is needed for differentiation. The QP problem in [2] is formulated as

$$y = \operatorname{argmin}_y \frac{1}{2} y^T Q y + q^T y \quad (15)$$

$$s.t. Ay = b, Gy \leq h,$$

where $Q, q, A, b, G,$ and h are parameters of the QP problem. These parameters are explicitly differentiable functions of the previous layers’ output x and are trainable just like other trainable parameters in the network. Q is constructed as a semi-positive definite matrix to ensure convexity.

The Lagrangian of (15) is

$$L(y, \lambda, \nu) = \frac{1}{2} y^T Q y + q^T y + \lambda^T (Ay - b) + \nu^T (Gy - h), \quad (16)$$

and the KKT conditions are

$$Qy^* + q + A^T \lambda^* + G^T \nu^* = 0$$

$$Ay^* - b = 0 \quad (17)$$

$$D(\nu^*)(Gy^* - h) = 0,$$

where operation $D(\cdot)$ diagonalise a vector.

(17) is the implicit-function system that we are after since it conforms with (4) by $y^{(k)} = [Q, q, A, b, G, h]$ and $y^{(k+1)} = y$.

Our implicit QP layer uses the same primal-dual interior point method to solve (15) as in [2] for the forward path, and apply (11) to (17) to get the partial derivatives required for the backward pass.

To validate the implicit layer, we run the pipeline for 15 epochs and observe converging loss and accuracy. The test accuracy achieves 98.14% upon termination. As shown in

²An example is provided in the supplementary material.

fig. 3, the implicit QP layer branch and the OptNet branch have almost identical learning curves as expected; this is because both forward and backward formulae are theoretically the same for the two branches.

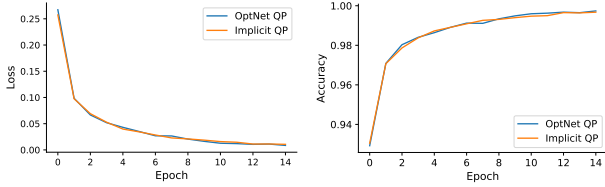


Figure 3: Hand written digits recognition learning curves.

The runtime comparison between the implicit QP layer and OptNet’s QP layer suggests the implicit QP layer falls behind with the backward computation; see fig. 4. This is to be expected as our current implementation is not optimised for speed.

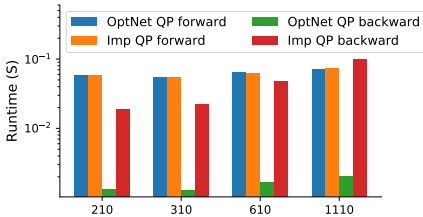


Figure 4: Runtime comparison between the implicit QP layer and OptNet’s QP layer. The x-axis represents the number of trainable parameters in the layer, and the y-axis indicates the runtime in seconds averaged over 500 trials on CPU.

4.2. QAP Layer for Graph Matching

A key contribution of our implicit layer technique lies in its generality. This section uses the application graph matching to demonstrate our implicit layer can differentiate through more general optimization problems while OptNet is incapable of, e.g., quadratic programming with quadratic constraints (QCQP) and maximizing a Rayleigh Quotient with affine constraints [8].

We borrow the graph matching pipeline from [34], which is also an end-to-end architecture that learns to match the landmarks on the source image to those on the target image. As shown in fig. 5, the pipeline starts with constructing two graphs for the source landmarks and the target landmarks respectively; meanwhile, a CNN backbone (e.g. VGG-16 [30]) extracts high-level features for the landmarks to establish landmark-to-landmark affinities and edge-to-edge affinities; this is followed by a layer that outputs the affinity matrix M between the two graphs based on the affinities

calculated in the previous layer. The optimal matching (assignment) y^* is then obtained by solving a QAP problem on M , formulated as:

$$y^* = \underset{y}{\operatorname{argmax}} y^T M y, \tag{18}$$

$$s.t. C y = 1, y \in \{0, 1\},$$

where the binary matrix C encodes one-to-one mapping constraints.

Since (18) is NP-hard, existing works often solve some relaxed type of the original problem. In what follows, we demonstrate 3 methods of solving 2 different types of relaxed QAP problem. The 3 methods are the Power Iteration (PI) method [34], the Spectral Matching (SM) method [8], and the Spectral Matching with Affine Constraints (SMAC) method [8]. Details about the SM method and the SMAC method are provided in the sec. 4.2.1 and sec. 4.2.2.

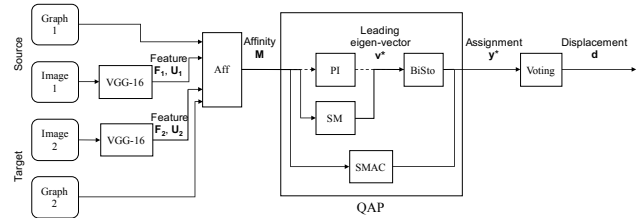


Figure 5: Graph matching pipeline. The VGG-16 extracts high level landmark features ($F1, F2, U1, U2$) to compute the affinity matrix M . Then the optimal matching y^* is gained for by solving a relaxed QAP problem on M . The Bi-stochastic layer produces a doubly-stochastic confidence map S from y^* . The voting layer converts from the confidence map S to the predicted displacement d . Refer to [34] for more details.

4.2.1 Solving QCQP

[34] drops both the binary and the mapping constraints on (18) and leads to the QCQP problem:

$$y^* = \underset{y}{\operatorname{argmax}} y^T M y, \tag{19}$$

$$s.t. \|y\|_2 = 1.$$

The method of matching two graphs by solving (19) is known as Spectral Matching (SM) method [8]. This comes from the fact that y^* the global optimiser of (19) is given by the leading eigenvector of matrix M . To be able to differentiate through (19), [34] employs the PI algorithm for eigen-decomposition since each iteration of PI is a differentiable operation, though the need to choose a maximum number of iterations is an inconvenience. With the implicit

layer technique, we are able to solve (19) with any eigen-decomposition algorithm and applying (11) to the KKT conditions (20) of (19) to prepare the necessary gradients:

$$\begin{aligned} My^* + \lambda^* I y^* &= 0 \\ y^{*T} y^* - 1 &= 0, \end{aligned} \quad (20)$$

with λ the dual variable and I the identity matrix.

We want to highlight in this example that the implicit QCQP layer uses different equations for the forward path and the backward path. It uses eigen-decomposition for the forward path (to guarantee optimality, a forward path based on KKT conditions only finds local optimum as the problem is in general not convex), and uses the KKT conditions as the backward equations. The independence between forward and backward equations adds to the flexibility of the implicit layer.

4.2.2 Maximizing a Rayleigh Quotient with Affine Constraints

Dropping only the binary constraints on (18) results in maximizing a Rayleigh Quotient with affine constraints [8]:

$$\begin{aligned} y^* &= \underset{y}{\operatorname{argmax}} \frac{y^T M y}{y^T y}, \\ \text{s.t. } C y &= 1, \quad y \geq 0 \quad (\equiv -I y \leq 0). \end{aligned} \quad (21)$$

The Lagrangian of (21) is

$$L(y, \lambda) = \frac{y^T M y}{y^T y} + \lambda^T (C y - 1) - \nu^T I y, \quad (22)$$

and the KKT conditions are

$$\begin{aligned} 2 \frac{M y^* y^{*T} y^* - y^{*T} M y^* I y^*}{(y^{*T} y^*)^2} + C^T \lambda^* - I \nu^* &= 0, \\ C y^* - 1 &= 0, \\ D(\nu^*) I y^* &= 0, \end{aligned} \quad (23)$$

which form the needed implicit-function system.

Matching graphs by solving (21) is called Spectral Matching with Affine Constraints (SMAC) algorithm. Incorporating the SMAC algorithm into the existing graph matching pipeline is easy. We simply construct an implicit SMAC layer and substitute it to the PI layer and the Bi-stochastic layer (the output of SMAC guarantees to be doubly-stochastic so it bypasses the Bi-stochastic layer in the pipeline), see the bottom solid branch of the pipeline in fig. 5. It would be otherwise cumbersome, if ever possible, for [34] to utilise SMAC algorithm in its original design.

The forward path can be performed by any numerical optimization toolbox, and we use SciPy package [1] in the

experiment. The differentiations in the backward path is also calculated by applying (11) to the KKT conditions (23) of (21).

We evaluate the implicit SM layer and the implicit SMAC layer on the CUB-200-2011 dataset [32]. The dataset contains 11,788 images of 200 bird species, with a total of 15 parts were annotated by pixel location and visibility in each image. Since the purpose of this experiment is to verify the prototype of implicit layer rather than to show a comprehensive competition with [34], we simplify the learning process in two ways. First, we use a subset of the CUB-200-2011 dataset that was built by [17]. The new dataset contains 5,000 images pairs comprising more than 50,000 ground truth matches, and we split it into training dataset and test dataset at a ratio of 9:1. Second, we match fixed 8 randomly selected landmarks across images instead of matching up to 15 landmarks. We report the percentage of correct keypoints (PCK) metric [33] where a match is considered correct if the prediction is within $\alpha \sqrt{w^2 + h^2}$ of the ground truth (w and h are respectively the width and height of input images). We use Delaunay triangulation to construct the graph structure on the source image and assign a fully connected graph to the target image.

Fig. 6 shows the accuracy increases with each iteration of training for all methods. Observe that implicit SMAC layer leads the PCK metric initially but eventually other methods catch up as the CNN backbone gradually learns to adapt to the specific choice of QAP methods.

Fig. 7 provides the runtime profile for the three branches. Fig. 8 shows qualitative results of the branch using the implicit SMAC layer.

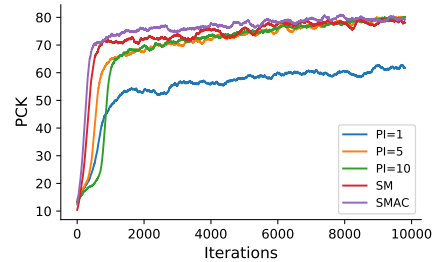


Figure 6: Graph matching learning curves. It plots the PCK against training iterations. $PI = k$ in the legend represents the PI layer with number of k iterations. We set $\alpha = 0.1$ in calculating PCK.

4.3. Normalised Cuts Segmentation Layer

Beyond finding the leading eigenvector (as in section 4.2.1), the implicit layer technique also allows us to defined layers involving generalised eigenvalues of any order. Solving arbitrary generalised eigenvector is useful in a range of image processing and computer vision tasks.

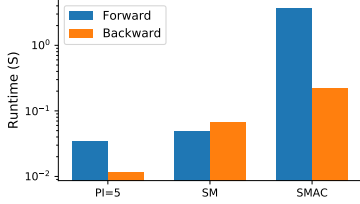


Figure 7: Runtime comparison of the implicit SM layer, the implicit SMAC layer, and the PI layer with 5 iterations.

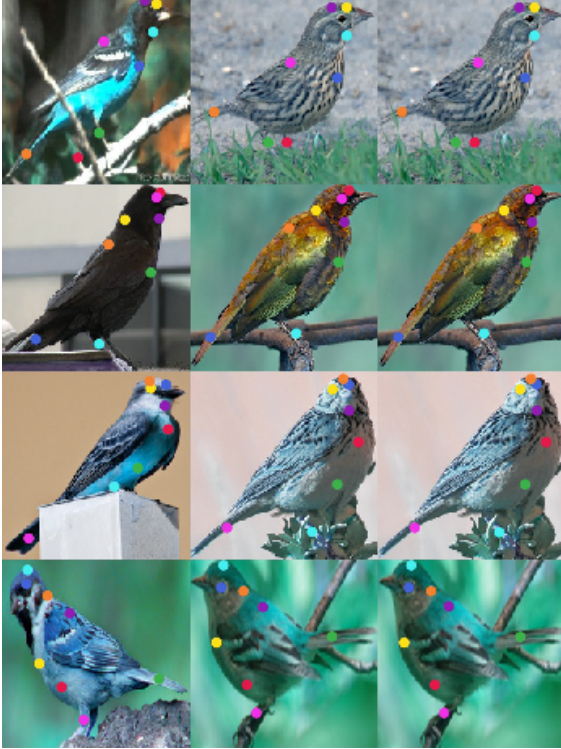


Figure 8: Qualitative results of the SMAC branch of the graph matching pipeline. Landmarks are color coded. For each example, the source image is on the left, the target image with predicted landmarks is in the middle, and on the right is the target image with ground truth landmarks.

A classical method for image segmentation is the Normalised Cuts (NCut) algorithm, [29]. This approach formulates the task of partitioning an image into foreground and background as a generalised eigenvalue problem. Specifically, as the problem of finding the generalised eigenvector of the second smallest generalised eigenvalue of the eigen-system

$$Lv = -\lambda Dv. \quad (24)$$

Here L denotes the Laplacian matrix of the adjacency matrix of the image and D is a diagonal matrix of the weighted

graph order, see [29] for further details. With the additional constraint that $v^T v = 1$, we can define our implicit NCut layer as

$$\begin{aligned} (L - \lambda_i D)v_i &= 0. \\ v_i^T v_i - 1 &= 0 \end{aligned} \quad (25)$$

The forward path of the implicit NCut layer is realised using standard eigensolvers.

To evaluate the implicit Ncut layer, we construct a simple network with an implicit NCut layer and compare it with the non-learning based Normalised Cut method, see fig. 9.

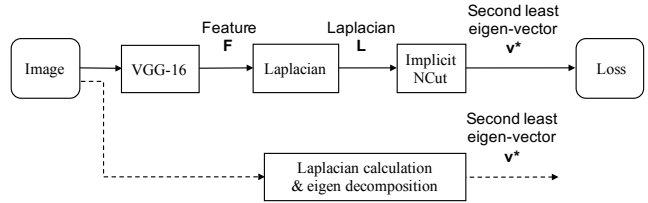


Figure 9: Spectral image segmentation pipeline. The solid branch uses the implicit NCut layer to decompose the Laplacian L , which is based on learned features. On the contrary, the Laplacian in NCut method (the dashed branch) is based on handcrafted features.

We evaluate the pipeline on the HazySky dataset [31] which contains 500 natural images with ground truth sky/non-sky segmentation mask. 400 images are randomly sampled as training data with the rest for testing. Fig. 10 shows loss and IOU converge, and the test IOU eventually plateaus at around 85%. In comparison, the non-learning based NCut method maintains a IOU score around 70%.

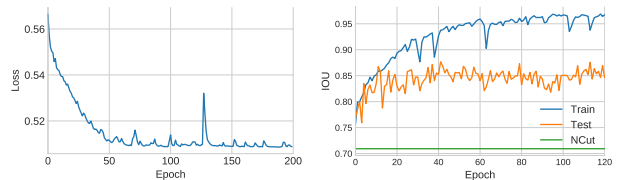


Figure 10: Normalised cuts segmentation learning curves. The left panel plots the loss against epochs, and the right panel compares the IOU score between the implicit NCut layer pipeline and the non-learning based NCut method.

4.4. Level-set Layers for Shape Inference

Representing shape in end-to-end trainable neural networks has proven to be challenging task. A majority of existing learning-based approaches involving shape or structure rely on either voxel occupancy [12, 7, 27, 28], sparse point clouds [26, 11] or explicit shape parameterisation

[20]. Each of these representations comes with its own advantages and disadvantages, in particular for the application of shape inference in a learning framework. Recent work [25, 23] has instead argued that *Level Sets* constitute a more appropriate choice for the task of learned shape inference.

The Level Set method for representing moving interfaces was proposed independently by [24] and [10]. This method defines a time dependent orientable surface $\Gamma(t)$ implicitly as the zero isocontour, or level set, of a higher dimensional auxiliary scalar function, called the *level set function* or *embedding function*, $\phi(x, t) : \Omega \times \mathbb{R} \mapsto \mathbb{R}$, as,

$$\Gamma(t) = \{x : \phi(x, t) = 0\}, \quad (26)$$

with the convention that $\phi(x, t)$ is positive on the interior and negative on the exterior of Γ . The underlying idea of the level set method is to capture the motion of the isosurface through the manipulation of the level set function ϕ .

However, owing to this implicit definition of shape, existing deep learning frameworks can not incorporate this representation straightforwardly. Instead, the inference is either carried out on the embedding function ϕ [25] directly, not on the shape itself, thus resulting in suboptimal reconstructions, or by approximating metrics on the iso-surfaces of ϕ [23].

In this section we will show how the level set representations can be included exactly using implicit layers. Again, the aim here is not provide an exhaustive study of implicit representations of shape but rather to demonstrate the applicability of our proposed framework.

The definition of the implicit layer that realises (26) is provided directly by its definition as $0 = \phi(x)$. However, here the input to this layer is a discrete representation of the embedding function ϕ and thm. 1 assumes a continuous function F . This can be accomplished by constructing a continuous surrogate of ϕ and using this to represent the desired implicit layer. We define

$$0 = \phi_{tri}(y^{(k+1)}; y^{(k)}) \quad (27)$$

as our implicit layer representation of (26). Here $\phi_{tri}; y^{(k)}$ denotes the trilinear interpolation of $y^{(k)}$ at $y^{(k+1)}$.

The forward pass through this layer can be obtained by any isosurface extraction algorithm, see [15]. In this setup we use standard marching cubes [21].

We followed the implementation details provided in [12] and [23] as closely as possible with respect to preprocessing, image rendering and evaluation. Our network was evaluated with the proposed formulation on 2,000 3D models from a single category ('cars') in the ShapeNet dataset [6]. The results, using a 32^3 resolution, are shown in figure 11 and table 1.

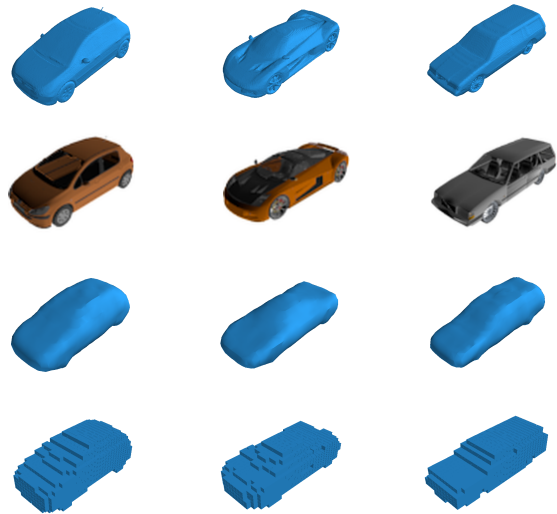


Figure 11: Shape inference from a single image. Ground truth (top), input image (second row) level sets (third row) voxels (bottom)

	IoU	Chamfer
Voxels	0.8144	0.0630
Level Sets	0.8680	0.0359

Table 1: Average test errors using voxels and level sets representations.

5. Conclusion

We presented a general framework of implicitly defined layers and showed its superior representation power to the standard explicit layers. We also established the backpropagation mechanism for implicit layers to utilise the Automatic Differentiation techniques in existing deep learning libraries and thus obviate the need to derive algebraic expressions of the differentiation. A number of diverse examples demonstrated the versatility of implicit layers. We hope this work could inspire the community to further explore and realise the potential of applying implicit function theories in the paradigms of machine learning.

A. An Example of Auto-differentiation

Let us consider the following simple example of an implicitly defined layer.

$$\begin{aligned} F_1(x, y) &= x^2 + y_1^2 + y_2^2 - 4, \\ F_2(x, y) &= xy_1 - 1. \end{aligned} \quad (28)$$

A solution to $F(x, y) = 0$ is given by $(\hat{x} = 1, \hat{y} = [1, \sqrt{2}])$. To calculate the backward pass, (i.e. the partial derivatives of the output y with respect to the input x) through such a layer we instead look at the related explicit layer defined by

$$z^{(k+1)} = F(z^{(k)}), \quad z^{(k)} \in \mathbb{R}^3, \quad z^{(k+1)} \in \mathbb{R}^2, \quad (29)$$

specifically where

$$\begin{aligned} z^{(k)} &= (x, y) = (\hat{x}, \hat{y}_1, \hat{y}_2), \\ z^{(k+1)} &= (0, 0). \end{aligned} \quad (30)$$

As this layer is defined explicitly, we can apply auto-differentiation directly to provide

$$\frac{\partial z_i^{(k+1)}}{\partial z_j^{(k)}}(z) = \frac{\partial F_i}{\partial z_j^{(k)}}(z), \quad i = 1, 2, \quad j = 1, 2, 3, \quad (31)$$

for some $z \in \mathbb{R}^3$, or more compactly as

$$J_{z^{(k+1)}, z^{(k)}}(z) = J_{F, z^{(k)}}(z). \quad (32)$$

In our simple example we have

$$\begin{aligned} J_{F, z^{(k)}}(z^{(k)}) &= \begin{bmatrix} \frac{\partial F_1}{\partial x} & \frac{\partial F_1}{\partial y_1} & \frac{\partial F_1}{\partial y_2} \\ \frac{\partial F_2}{\partial x} & \frac{\partial F_2}{\partial y_1} & \frac{\partial F_2}{\partial y_2} \end{bmatrix} = [J_{F, x}(z^{(k)}) \mid J_{F, y}(z^{(k)})] \\ &= \begin{bmatrix} 2x & 2y_1 & 2y_2 \\ y_1 & x & 0 \end{bmatrix} = \begin{bmatrix} 2 & 2 & 2\sqrt{2} \\ 1 & 1 & 0 \end{bmatrix}. \end{aligned} \quad (33)$$

Finally,

$$\begin{aligned} J_{y, x}([\hat{x}, \hat{y}]) &= -[J_{F, y}([\hat{x}, \hat{y}])]^{-1} [J_{F, x}([\hat{x}, \hat{y}])] = \\ &= - \begin{bmatrix} 2 & 2\sqrt{2} \\ 1 & 0 \end{bmatrix}^{-1} \begin{bmatrix} 2 \\ 1 \end{bmatrix} \end{aligned} \quad (34)$$

Recall that as (33) is calculated by auto-differentiation, so we eventually get the partial derivative $J_{y, x}$ of the output y of the implicit layer with respect to the input x without manually deriving algebraic expressions of the differentiation.

References

- [1] scipy.optimize.minimize. <https://docs.scipy.org/doc/scipy/reference/generated/scipy.optimize.minimize.html>.
- [2] Brandon Amos and J Zico Kolter. Optnet: Differentiable optimization as a layer in neural networks. In *Proceedings of the 34th International Conference on Machine Learning-Volume 70*, pages 136–145. JMLR. org, 2017.
- [3] Brandon Amos, Lei Xu, and J Zico Kolter. Input convex neural networks. In *Proceedings of the 34th International Conference on Machine Learning-Volume 70*, pages 146–155. JMLR. org, 2017.
- [4] J Frédéric Bonnans and Alexander Shapiro. *Perturbation analysis of optimization problems*. Springer Science & Business Media, 2013.
- [5] Rainer E Burkard, Eranda Cela, Panos M Pardalos, and Leonidas S Pitsoulis. The quadratic assignment problem. In *Handbook of combinatorial optimization*, pages 1713–1809. Springer, 1998.
- [6] Angel X Chang, Thomas Funkhouser, Leonidas Guibas, Pat Hanrahan, Qixing Huang, Zimo Li, Silvio Savarese, Manolis Savva, Shuran Song, Hao Su, et al. Shapenet: An information-rich 3d model repository. *arXiv preprint arXiv:1512.03012*, 2015.
- [7] Christopher B Choy, Danfei Xu, JunYoung Gwak, Kevin Chen, and Silvio Savarese. 3d-r2n2: A unified approach for single and multi-view 3d object reconstruction. In *European conference on computer vision*, pages 628–644. Springer, 2016.
- [8] Timothee Cour, Praveen Srinivasan, and Jianbo Shi. Balanced graph matching. In *Advances in Neural Information Processing Systems*, pages 313–320, 2007.
- [9] Daniel Cremers, Mikael Rousson, and Rachid Deriche. A review of statistical approaches to level set segmentation: integrating color, texture, motion and shape. *International journal of computer vision*, 72(2):195–215, 2007.
- [10] Alain Dervieux and François Thomasset. A finite element method for the simulation of a rayleigh-taylor instability. In *Approximation methods for Navier-Stokes problems*, pages 145–158. Springer, 1980.
- [11] Haoqiang Fan, Hao Su, and Leonidas J Guibas. A point set generation network for 3d object reconstruction from a single image. In *Proceedings of the IEEE Conference on Computer Vision and Pattern Recognition.*, volume 2, page 6, 2017.
- [12] Rohit Girdhar, David F Fouhey, Mikel Rodriguez, and Abhinav Gupta. Learning a predictable and generative vector representation for objects. In *European Conference on Computer Vision*, pages 484–499. Springer, 2016.
- [13] Stephen Gould, Basura Fernando, Anoop Cherian, Peter Anderson, Rodrigo Santa Cruz, and Edison Guo. On differentiating parameterized argmin and argmax problems with application to bi-level optimization. *arXiv preprint arXiv:1607.05447*, 2016.
- [14] A. G. Hamilton. *Numbers, Sets and Axioms: The Apparatus of Mathematics*. Cambridge University Press, 1983.
- [15] Charles D Hansen and Chris R Johnson. *Visualization handbook*. Elsevier, 2011.
- [16] Matthew J Johnson, David K Duvenaud, Alex Wiltschko, Ryan P Adams, and Sandeep R Datta. Composing graphical models with neural networks for structured representations and fast inference. In *Advances in neural information processing systems*, pages 2946–2954, 2016.
- [17] Angjoo Kanazawa, David W Jacobs, and Manmohan Chandraker. Warpnet: Weakly supervised matching for single-view reconstruction. In *Proceedings of the IEEE Conference on Computer Vision and Pattern Recognition*, pages 3253–3261, 2016.
- [18] Steven G Krantz and Harold R Parks. *The implicit function theorem: history, theory, and applications*. Springer Science & Business Media, 2012.
- [19] Karl Kunisch and Thomas Pock. A bilevel optimization approach for parameter learning in variational models. *SIAM Journal on Imaging Sciences*, 6(2):938–983, 2013.
- [20] Yiyi Liao, Simon Donné, and Andreas Geiger. Deep marching cubes: Learning explicit surface representations. In *Proceedings of the IEEE Conference on Computer Vision and Pattern Recognition*, pages 2916–2925, 2018.
- [21] William E Lorensen and Harvey E Cline. Marching cubes: A high resolution 3d surface construction algorithm. In *ACM siggraph computer graphics*, volume 21, pages 163–169. ACM, 1987.
- [22] Julien Mairal, Francis Bach, and Jean Ponce. Task-driven dictionary learning. *IEEE transactions on pattern analysis and machine intelligence*, 34(4):791–804, 2011.
- [23] Mateusz Michalkiewicz, Jhony K. Pontes, Dominic Jack, Mahsa Baktashmotlagh, and Anders Eriksson. Implicit surface representations as layers in neural networks. In *The IEEE International Conference on Computer Vision (ICCV)*, October 2019.
- [24] Stanley Osher and James A Sethian. Fronts propagating with curvature-dependent speed: algorithms based on hamilton-jacobi formulations. *Journal of computational physics*, 79(1):12–49, 1988.
- [25] Jeong Joon Park, Peter Florence, Julian Straub, Richard Newcombe, and Steven Lovegrove. DeepSDF: Learning continuous signed distance functions for shape representation. In *The IEEE Conference on Computer Vision and Pattern Recognition (CVPR)*, June 2019.
- [26] Charles R Qi, Hao Su, Kaichun Mo, and Leonidas J Guibas. Pointnet: Deep learning on point sets for 3d classification and segmentation. *Proceedings of the IEEE Conference on Computer Vision and Pattern Recognition.*, 1(2):4, 2017.
- [27] Danilo Jimenez Rezende, SM Ali Eslami, Shakir Mohamed, Peter Battaglia, Max Jaderberg, and Nicolas Heess. Unsupervised learning of 3d structure from images. In *Advances in Neural Information Processing Systems*, pages 4996–5004, 2016.
- [28] Stephan R Richter and Stefan Roth. Matryoshka networks: Predicting 3d geometry via nested shape layers. In *Proceedings of the IEEE Conference on Computer Vision and Pattern Recognition*, pages 1936–1944, 2018.
- [29] Jianbo Shi and Jitendra Malik. Normalized cuts and image segmentation. *IEEE Transactions on Pattern Analysis and Machine Intelligence*, 2000.

- [30] Karen Simonyan and Andrew Zisserman. Very deep convolutional networks for large-scale image recognition. *arXiv preprint arXiv:1409.1556*, 2014.
- [31] Yingchao Song, Haibo Luo, Junkai Ma, Hui Bin, and Zhenxing Chang. Sky detection in hazy image. *Sensors*, 18:1060, 04 2018.
- [32] C. Wah, S. Branson, P. Welinder, P. Perona, and S. Belongie. The Caltech-UCSD Birds-200-2011 Dataset. Technical Report CNS-TR-2011-001, California Institute of Technology, 2011.
- [33] Yi Yang and Deva Ramanan. Articulated pose estimation with flexible mixtures-of-parts. In *CVPR 2011*, pages 1385–1392. IEEE, 2011.
- [34] Andrei Zanfir and Cristian Sminchisescu. Deep learning of graph matching. In *Proceedings of the IEEE Conference on Computer Vision and Pattern Recognition*, pages 2684–2693, 2018.